Plasma-catalytic methanol synthesis from CO_2 hydrogenation over a supported Cu cluster catalyst : insights into the reaction mechanism

Plasma-catalytic Methanol Synthesis from CO_2 Hydrogenation over Supported Cu cluster Catalyst: Insights into the Reaction Mechanism

Zhaolun Cui[a,b,⊥], Shengyan Meng[c,⊥], Yanhui Yi[b, c,*], Amin Jafarzadeh[b], Shangkun Li[b,c], Erik C Neyts[b], Yanpeng Hao[a], Licheng Li[a], Xiaoxing Zhang[d,*], Xinkui Wang[c], Annemie Bogaerts[b]

[a] School of Electric Power Engineering, South China University of Technology, Guangzhou 510630, China

[b] Research group PLASMANT, Department of Chemistry, University of Antwerp, Universiteitsplein 1, BE-2610 Wilrijk-Antwerp, Belgium

[c] State Key Laboratory of Fine Chemicals, School of Chemical Engineering, Dalian University of Technology, Dalian 116024, P.R. China

[d] School of Electrical and Electronic Engineering, Hubei University of Technology, Wuhan, 430068, China

Email: yiyanhui@dlut.edu.cn

Email: xiaoxingzhang@outlook.com

⊥: Z. Cui and S. Meng contributed equally to this paper

ABSTRACT: Plasma-catalytic CO_2 hydrogenation for methanol production is gaining increasing interest, but our understanding of its reaction mechanism remains primitive. We present a combined experimental/computational study on plasma-catalytic CO_2 hydrogenation to CH_3OH over a size-selected $Cu/\gamma\text{-}Al_2O_3$ catalyst. Our experiments demonstrate a synergistic effect between the $Cu/\gamma\text{-}Al_2O_3$ catalyst and the CO_2/H_2 plasma, achieving a CO_2 conversion of 10% at 4 wt.% Cu loading and a CH_3OH selectivity near 50%, further rising to 65% with H_2O addition (for a H_2O/CO_2 ratio of 1). Furthermore, the energy consumption for CH_3OH production was more than 20 times lower than with plasma-only. We carried out DFT calculations over a $Cu_{13}/\gamma\text{-}Al_2O_3$ model, which reveal that the interface sites of the Cu_{13} cluster and $\gamma\text{-}Al_2O_3$ support show a bifunctional effect: they do not only activate the CO_2 molecules but also strongly adsorb key intermediates to promote their further hydrogenation. Reactive plasma species can regulate the catalyst surface reactions via the Eley–Rideal (E-R) mechanism, which accelerates the hydrogenation process and promotes the generation of the key intermediates. H_2O can promote the CH_3OH desorption by competitive adsorption over the $Cu_{13}/\gamma\text{-}Al_2O_3$ surface. This study gives new insight in CO_2 hydrogenation through plasma catalysis and it provides inspiration for the conversion of some other small molecules (CH_4, N_2, CO, etc.) by plasma catalysis using supported-metal clusters.

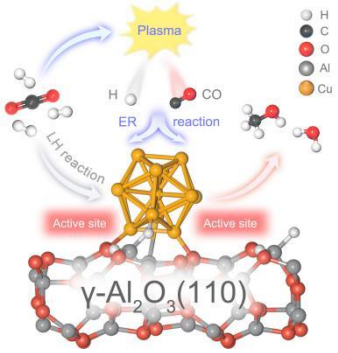

KEYWORDS: Non-thermal plasma; Catalysis; CO_2; CH_3OH; Hydrogenation; $Cu_{13}/\gamma\text{-}Al_2O_3$

1. INTRODUCTION

Increasing emission of carbon dioxide (CO_2) has resulted in more and more severe greenhouse effects, causing global climate changes. Therefore, extensive efforts have been devoted to CO_2 storage and utilization.[1,2] Among them, hydrogenation to CH_3OH is a promising way to utilize CO_2.[3, 4] Due to the high activity of a Cu surface, Cu-based catalysts have attracted considerable interest[5-7] and Cu particles combined with different promoters and supports showed synergistic effects in CO_2 conversion and CH_3OH selectivity.[8-10] For instance, a $Cu/ZnO/Al_2O_3$ catalyst is widely used in the chemical industry for CH_3OH synthesis with high CH_3OH selectivity and excellent catalytic stability.[11-13]

In recent years, supported metal cluster (SMC) catalysts are gaining great interests as they have advantages like high activity and high atom economy, and they show great catalytic potentials.[14] Liu et al. proved that size-selected Cu_4 clusters supported on an Al_2O_3 support have a promising activity for CH_3OH formation at a low CO_2 partial pressure.[15] However, the catalytic mechanism of supported Cu cluster catalysts for CO_2 hydrogenation to CH_3OH remains poorly understood.

CH_3OH synthesis by CO_2 hydrogenation is favored at low temperature and high pressure, as the reaction is exothermic and the number of molecules decreases upon the reaction. However, low-temperature operation suffers from a kinetic limitation in CO_2 activation, in contrast to the thermodynamic limitation of the reaction at high temperatures. In addition, high-pressure operation brings challenges for the reduction of energy cost. In 2018, Wang et al. demonstrated CO_2 hydrogenation to CH_3OH by non-thermal plasma (NTP) over $Cu/\gamma\text{-}Al_2O_3$ catalysts at atmospheric pressure and room temperature.[16] Indeed, highly energetic electrons in the plasma create radicals, which may help to overcome the activation barriers via the Eley–Rideal (E-R) mechanism, as compared to thermal catalysis.[17-19]

In recent years, plasma-assisted heterogeneous catalysis, simply called “plasma catalysis”, has been applied in C1

chemistry and has attracted more and more attention.[20-25] Various 'plasma effects' prove to be beneficial for CO_2 conversion and product yields, which makes plasma catalysis an attractive alternative to thermal catalysis. Therefore, in this paper, we want to explore whether a combination of a Cu cluster catalyst and plasma shows a synergistic effect for CO_2 hydrogenation to CH_3OH.

One of the challenges in plasma catalysis is to gain deeper insight in the synergistic effects between plasma and catalysts. Indeed, the underlying mechanisms in plasma catalysis remain poorly understood. Most of the modeling works focus on macroscopic (chemical kinetics and fluid) models,[26-28] while simulations at the molecular level are scarce. Nevertheless, the density functional theory (DFT) method is a promising way to provide valuable information on the reaction paths in catalysis.[26] DFT studies on thermal catalysis revealed that there are two main paths for CO_2 hydrogenation to CH_3OH, i.e., the formate (HCOO) path and the reverse water gas shift (RWGS) + CO-Hydro path (COOH path).[13,15,29,30] In the HCOO path, the hydrogenation of CO_2 proceeds through H_2COOH* or HCOOH* to H_2CO*, and finally it forms CH_3OH.[31,32] In the COOH path, CO_2 is first converted to CO* via COOH* through the RWGS reaction, and then CO* is converted to CH_3OH by further hydrogenation through HCO*, H_2CO* and H_2COH* or H_3CO*.

In the present study, we focus on supported Cu cluster catalysts for CO_2 hydrogenation into CH_3OH by plasma catalysis, by means of both experiments and DFT calculations. Our experiments demonstrate that γ-Al_2O_3 supported Cu cluster catalysts can significantly improve the production of CH_3OH and reduce the generation of CH_4, with an optimal CH_3OH selectivity reaching 65%. To understand the underlying mechanisms, we performed DFT calculations. We first investigated the reaction pathways for CH_3OH formation via the L-H mechanism. Subsequently, we considered the effects of plasma species participating via the E-R mechanism. Our DFT calculations reveal that the catalytic effects of Cu_{13}/γ-Al_2O_3 (110) are different from a Cu (111) plane slab or a single Cu cluster studied before, due to the metal-support interaction.[33,34] In the hydrogenation process, the RWGS and formate path are comparable in rate-limiting steps for CH_3OH formation via the L-H mechanism. Taking the plasma species into account, the overall hydrogenation barrier is much lower than in the L-H path, due to the E-R reactions. The RWGS path is found to be more significant in the case of plasma catalysis, since abundant CO molecules are produced and they can promote HCO* generation. Moreover, we found that H_2O facilitates the methanol yield due to its assistance of CH_3OH desorption. This study indicates the potential of plasma catalysis with Cu cluster catalysts for CO_2 hydrogenation to CH_3OH, and is in general important for a better understanding of plasma catalysis and its applications, especially with SMC catalysts.

2. MATERIALS AND METHODS

2.1 Preparation of the Cu/γ-Al_2O_3 Catalyst. The Cu/γ-Al_2O_3 catalysts with various loadings (1, 2, 3, 4 and 5 wt.%) are prepared by the incipient-wetness impregnation method. To remove water and impurities, the γ-Al_2O_3 support is calcined in a muffle furnace at 813K for 4 hours in air atmosphere. First, the precursor salt, i.e., $Cu(NO_3)_2 \cdot 5H_2O$, is dissolved in deionized water with varied concentrations based on the desired loading. Then, the support is added to the solution, and the mixture is stirred at ambient temperature for 30 minutes, followed by 15 hours aging and overnight drying at 393 K in air. After that, the samples are calcined at 673K for 5 hours, and finally the obtained samples are crushed and sieved to granules in a mesh range of 20-40 (0.85-0.42 mm diameter). Prior to catalytic tests, the samples are reduced by H_2 plasma (40 mL/min H_2, 26 W, 573 K) for one hour at atmospheric pressure.

2.2 Experimental Steps and Reaction Evaluation. A schematic diagram of the experimental equipment for the plasma-catalytic CO_2/H_2 reaction is shown in the supporting information (SI); Fig. S1. A coaxial dielectric barrier discharge (DBD) reactor is used to generate CO_2/H_2 plasma. The DBD reactor consists of a pair of coaxial quartz cylinders (inner and outer quartz tubes) in which a stainless-steel (2 mm outer diameter) electrode is placed in the center, and circulating water is pumped into the space between the inner and outer cylinder, acting as a ground electrode. The discharge length is 60 mm and the discharge gap is fully packed by catalyst granules (0.85-0.42 mm diameter). CO_2 (18 mL/min) and H_2 (54 mL/min) are monitored by calibrated mass flow controllers and mixed homogeneously with water vapor before passing through the plasma reactor. Indeed, water vapor is added (up to H_2O/CO_2 molar ratios of 1) to investigate its effect on the CO_2 conversion and CH_3OH selectivity. The water vapor is generated by a steam generator (FD-HG from Furande equipment Co., Ltd.). The discharge frequency is fixed at 9.5 kHz, and the applied power is maintained at around 26 W. The liquid product is collected by a cold trap at the exhaust of the DBD reactor. A gas chromatograph (Tianmei 7890 II equipped with a thermal conductivity detector and a TDX-01 column) is used to analyze the composition of the exhaust gases. The liquid products are quantitatively analyzed by another gas chromatograph (Shimadzu GC-2014C equipped with a flame ionization detector and a PEG-20M column). The variation of the gas volume is measured by a soap-film flow meter. The exhaust gas is analyzed online by a mass spectrometer (Pfeiffer Vacuum GSD301) with Faraday detection mode. The reaction temperature in the discharge area is close to the circulating water temperature (ca. 60 °C), while the temperature near the high-voltage electrode may be slightly higher than 60 °C .[16]

To evaluate the reaction performance, the CO_2 conversion is calculated by Eq (1),

$$X_{CO_2} = \frac{CO_{2[in]} - CO_{2[out]}}{CO_{2[in]}} \times 100\% \quad (1)$$

In the tail gas, only CO and CH_4 are detected by the gas chromatograph. The selectivity of CO and CH_4 is calculated by Eq (2) and Eq (3), respectively,

$$S_{CO} = \frac{CO_{[out]}}{CO_{2[in]} - CO_{2[out]}} \times 100\% \quad (2)$$

$$S_{CH_4} = \frac{CH_{4[out]}}{CO_{2[in]} - CO_{2[out]}} \times 100\% \quad (3)$$

In the collected liquid, only one single product, CH_3OH, is detected by our gas chromatograph. Thus, the selectivity of CH_3OH is calculated by Eq (4),

$$S_{CH_3OH} = 1 - S_{CO} - S_{CH_4} \quad (4)$$

The energy consumption for CH_3OH generation is

calculated by Eq (5),

$$energy\ consumption\ (kJ/mmol) = \frac{discharge\ power\ (J/s)}{rate\ of\ CH_3OH\ produced\ (mol/s)} \times 10^{-6} \quad (5)$$

where the factor 10^{-6} accounts for the conversion of J/mol into kJ/mmol.

2.3 Catalyst characterization. The crystal structure of the catalyst is determined by using Cu Kα radiation (40 kV, 50 mA) on a Rigaku D/Max2400 powder X-ray diffractometer, and the sample is scanned from 10° to 80° at a step of 10°/min. High-angle annular dark-field scanning transmission electron microscopy (HAADF-STEM) and elementary mapping are performed on a JEM-ARM200F electron microscope at 200 kV. The specific surface area, pore volume and pore size of the catalysts are measured by N_2 physisorption (Micromeritics ASAP 3020). Prior to the measurements, the catalysts are vacuum-treated at 623 K for 5 h to remove impurities adsorbed in the catalyst pores. The reduction properties of the catalysts are determined using H_2 temperature-programmed reduction (H_2-TPR) on a Quanta chrome ChemBET Pulsar TPR apparatus. The samples (0.15 g) are purged for 1 h at 723 K under He atmosphere. After cooling to room temperature, the samples are heated from room temperature to 773 K in an Ar-H_2 (120 mL/min, 10% H_2) atmosphere at a rate of 10 K/min, and the signal of H_2 consumption is collected. X-ray photoelectron spectroscopy (XPS) is performed on an ESCALAB250 instrument (ThermoVG, USA) with an Al Kα X-ray source.

2.4 Optical emission spectrometry. A Princeton Instruments ICCD spectrometer (SP 2758) with a 300 g/mm grating is used to in-situ diagnose the CO_2/H_2 plasma (200-1200 nm). The slit width of the spectrometer is fixed at 20 μm, and the exposure time is fixed at 2s.

2.5 Computational details. All DFT calculations are carried out in CP2K 7.0 package.[35] The Gaussian and plane wave (GPW) method in Quickstep module is applied to calculate the energies and forces.[36,37] The molecularly optimized (MOLOPT) double-ζ valence plus polarization (m-DZVP) basis set is used, combined with a 600 Ry cutoff set for the plane wave calculation. Goedecker-Teter-Hutter pseudopotentials are applied to treat the inner shell electrons.[38,39] The Perdew-Burke-Ernzerhof (PBE) functional in generalized gradient approximation (GGA) is chosen to describe the exchange correlation energy.[40] For dispersion correction, Grimme's D3 method with Becke-Johnson damping is applied.[41] The Broyden-Fletcher-Goldfarb-Shanno scheme is used for the geometry optimization.[42]

The k-point sampling is limited to the Γ point only. The atomic charge analysis is calculated by the Bader scheme.[43] The transition state (TS) calculations are carried out by the climbing image nudged elastic band (CI-NEB) method.[44] Vibrational analysis is carried out for the transition state validation to ensure there is only one imaginary frequency in each TS structure.

The widely used γ-Al_2O_3(110) surface is chosen to be the support slab.[45] It is modeled as a 2×2 supercell and contains 4 layers and 160 atoms. This structure has been used as a support for Ni cluster adsorption to activate CO_2 molecules.[46] The bottom two layers are fixed during the whole calculation. The simulation cell dimensions are 16.1439×16.7874×40.0000 $Å^3$ with a periodic boundary along XYZ directions.

As for the γ-Al_2O_3 surface termination, the 'dry' γ-Al_2O_3 (110) surface is not very stable and often hydrated (pre-adsorbed H and OH).[47] Besides, in plasma catalysis with H_2 gas involved, the plasma offers plenty of H atoms to adsorb on the catalyst surface, known as the 'net effect'.[48] Therefore, in this model, we placed 8 H atoms instead of 4 H and 4 OH on the γ-Al_2O_3 (110) surface, and the adsorption sites for H atoms are set the same as the H and OH sites for a 'hydrated' γ-Al_2O_3(110) surface.[47,49] After this treatment, the H-coverage ratio for γ-Al_2O_3 surface is 0.125 ML. The further investigation for the net effect and the H-coverages on the CO_2 hydrogenation process is out of scope and is not discussed in this paper.

The adsorption energy (E_{ad}) of the Cu_{13} cluster on the γ-Al_2O_3 surface is calculated by Eq (6),

$$E_{ad} = E_{slab+cluster} - E_{slab} - E_{cluster} \quad (6)$$

where E_{slab} and $E_{cluster}$ are the total energies of the γ-Al_2O_3 slab and Cu_{13} cluster, respectively, and $E_{slab+cluster}$ is the total energy of the Cu_{13} cluster adsorbed on the γ-Al_2O_3 system.

The adsorption energy of gas molecules on the Cu_{13}/γ-Al_2O_3 surface is calculated by Eq (7),

$$E_{ad} = E_{gas+complex} - E_{gas} - E_{complex} \quad (7)$$

where E_{gas} and $E_{complex}$ are the energies of gas molecules and of the Cu_{13}/γ-Al_2O_3 system, respectively and $E_{gas+complex}$ is the total energy of the gas molecules adsorbed on the Cu_{13}/γ-Al_2O_3 system. The binding energy (BE) of the intermediates on the Cu_{13}/γ-Al_2O_3 interface is also calculated by Eq (7), where E_{gas} is replaced by the energy of the intermediates, like COOH, HCOO and so on.

3. RESULTS AND DISCUSSION

3.1 Measured product selectivity, CO_2 conversion and energy consumption. Fig.1 shows the CO_2 hydrogenation results over a Cu/γ-Al_2O_3 catalyst. As illustrated in Fig. 1(a), in the absence of plasma, the CO_2 conversion is zero, indicating that CO_2 cannot be converted under room temperature and atmospheric pressure without the assistance of plasma. In the case of plasma-only, the CO_2 conversion reaches 6.1%, but with only 3.7% CH_3OH selectivity. After packing the CO_2/H_2 plasma with γ-Al_2O_3, the CO_2 conversion and CH_3OH selectivity increase to 7.6% and 17.4%, respectively, while adding the Cu/γ-Al_2O_3 catalyst (4 wt.% loading) yields a further increase in the performance: the CO_2 conversion and CH_3OH selectivity increase to 9.8% and 47.5%, respectively. These results demonstrate that the Cu/γ-Al_2O_3 catalyst has a synergistic effect with plasma, resulting in a high activity toward CO_2 conversion and CH_3OH synthesis.

Fig. 1(b) shows the performance of the Cu/γ-Al_2O_3 catalysts with various loadings. The CO_2 conversion and CH_3OH selectivity first increase and then decrease upon increasing Cu loading, and the optimum loading is 4 wt.% at these experimental conditions.

In addition, we investigated the influence of H_2O on the CH_3OH synthesis, as shown in Fig. 1(c). With increasing H_2O/CO_2 molar ratio from 0:1 to 1:1, the CH_3OH selectivity increases from 47.5% to 65.2%, while the CO selectivity decreases from 51.4% to 33.6%. The CO_2 conversion, on the

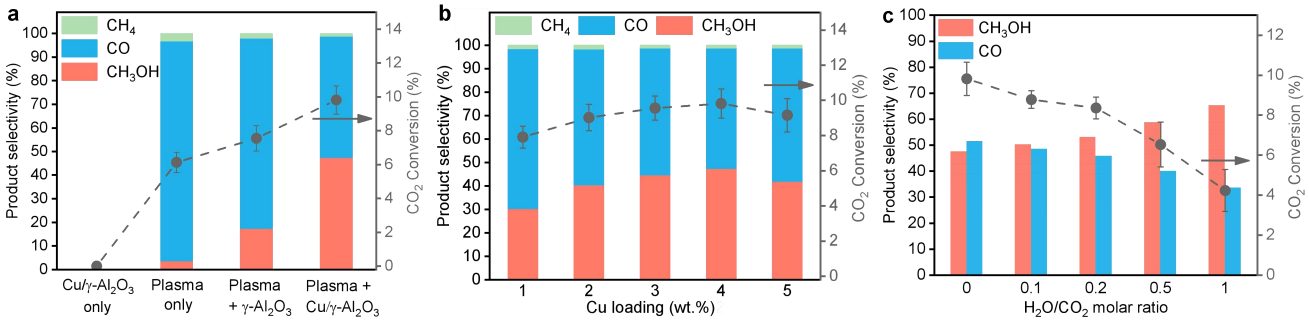

Fig. 1 Measured product selectivity and CO_2 conversion for CO_2 hydrogenation over Cu/γ-Al_2O_3 catalyst: (a) For catalysis-only (CO_2:H_2 = 1:3, WHSV = 2400 mL/g/h), plasma-only, and plasma catalysis with γ-Al_2O_3 and 4% Cu/γ-Al_2O_3 catalyst (CO_2:H_2 = 1:3, WHSV = 2400 mL/g/h, 26 W input power). (b) For plasma catalysis with different Cu loading (CO_2:H_2 = 1:3, WHSV = 2400 mL/g/h, 26 W input power). (c) For plasma catalysis with different H_2O/CO_2 molar ratios (total CO_2/H_2 flow rate = 72 mL/min with 1:3 ratio)

other hand, drops upon H_2O addition, which is attributed to the competitive adsorption on the active sites, as will be shown by our DFT calculations. Furthermore, Fig.S2 shows that a high content of H_2O reduces the discharge voltage and current. It's clear that when the H_2O/CO_2 ratio rises from 1.0 to 1.5, the discharge voltage as well as the current are more significantly reduced. This could also be a possible reason for the lower CO_2 conversion presented in Fig. 1(c).

To understand the role of H_2O in improving the CH_3OH selectivity, we analyzed the exhaust gas during reaction by online mass spectrometry. As shown in Fig. S3, after switching on the plasma, the signal intensity of *CH_3O increases, which represents the production of CH_3OH. Interestingly, a sharp increase of the *CH_3O signal is observed after each H_2O injection, indicating that more CH_3OH is produced after adding H_2O to the feedstock. This experimental result can be explained by the promoting function of H_2O in CH_3OH desorption, as revealed by our DFT calculations (see section 3.7 below), as well as in literature studies.[50-52]

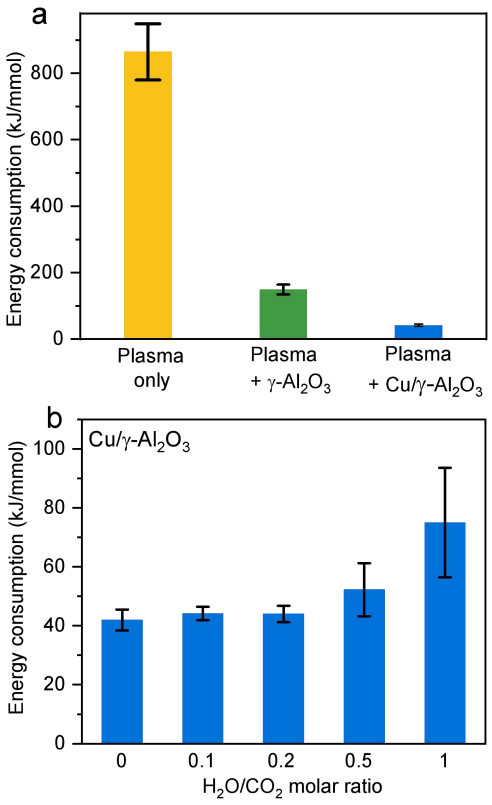

Fig. 2 Energy consumption for CH_3OH generation: (a) for plasma-only, plasma + γ-Al_2O_3 and plasma + Cu/γ-Al_2O_3, and (b) for plasma catalysis with different H_2O/CO_2 molar ratios.

Note that we also performed experiments in a CO_2/H_2O plasma (both in the absence and presence of Cu/γ-Al_2O_3 catalyst). Indeed, H_2O vapor could be an interesting source of H, as also demonstrated by Gorbanev et al. for another application, i.e., catalyst-free and H_2-free NH_3 synthesis from N_2/H_2O mixtures.[53] However, in our experiments the measured CO_2 conversion in the CO_2/H_2O plasma was nearly zero, and no CH_3OH was detected in the collected liquid. This corresponds well with an earlier paper by Snoeckx et al., where the drop in CO_2 conversion upon addition of H_2O vapor, as well as the absence of CH_3OH formation, was explained by chemical kinetics modeling, i.e., more specifically due to the recombination reaction of CO with OH radicals, forming again CO_2.[54] In addition, Zhao et al. obtained CH_3OH and CH_3CH_2OH using a CO_2/H_2O plasma, but the yields were only in the μmol level.[55]

The energy consumption is also a key indicator for plasma catalysis. We present the energy consumption of CH_3OH generation at different conditions in Fig. 2. It is clear that the energy efficiency is significantly improved by combining the plasma and the Cu/γ-Al_2O_3 catalyst, as the energy consumption drops from 855.9 kJ/mmol in the plasma-only system to 147.7 kJ/mmol in the plasma + γ-Al_2O_3 system and eventually it drops to 41.6 kJ/mmol in the plasma + Cu/γ-Al_2O_3 system, as shown in Fig.2(a). This reduction in energy consumption by more than a factor of 20 indicates the key role of the active metal (Cu cluster) for efficiently producing CH_3OH. On the other hand, in Fig. 2(b) we show that increasing the H_2O concentration enlarges the energy consumption, indicating that its negative impact on CO_2 conversion is stronger than its promotion effect on CH_3OH generation.

Furthermore, under all conditions, the CH_4 selectivity remains at a low level (< 2%), which is in line with literature, showing a hindering effect of Cu-based catalysts on CH_4 yields.[15] This will be explained in our DFT results, due to the high activation barriers for CH_4 production (see section 3.5 below).

Table S1 in the SI compares our results (for plasma catalysis) with some representative results from literature for conventional thermal catalysis. It is clear that our plasma catalysis experiments exhibit a similar degree of CO_2 conversion as conventional thermal catalysis. The selectivity

towards CH_3OH in our plasma catalysis experiments is a little lower than in conventional thermal catalysis, which is attributed to the high reactivity of the CO_2/H_2 plasma, leading also to production of CO through the RWGS reaction. With regard to the reaction conditions, conventional thermal catalysis generally needs to be operated at higher temperature (180-300 °C) and higher pressure (0.5-36 MPa), while plasma catalysis can be operated at ambient temperature and atmospheric pressure, which is the main advantage compared to conventional thermal catalysis. Finally, the energy consumption is also presented in Table S1, but since the data of conventional thermal catalysis are expressed in different units, we could not compare the energy consumption between plasma catalysis and thermal catalysis.

3.2 In-situ OES to detect the important plasma species in the CO_2/H_2 plasma. We applied in-situ optical emission spectroscopy (OES) to detect the important species in the CO_2/H_2 plasma, as presented in Fig. 3. The CO_2/H_2 plasma in the absence of catalyst or support shows the highest signal intensity, including several spectral lines and two spectral bands: the H_α line[56] (656.3 nm, $3d^2D \rightarrow 2p^2P^0$), two O atomic spectral lines[57,58] (777.5 nm, $3s^5S^0 \rightarrow 3p^5P$; 844.7 nm, $3s^3S^0 \rightarrow 3p^3P$), a H_2 band (580-650 nm, $d^3\Pi_u \rightarrow a^3\sum_g^+$) and a CO band (450-580 nm, $B^1\sum \rightarrow A^1\Pi$).[59] This indicates that H atoms and CO molecules are abundantly produced in the plasma region.

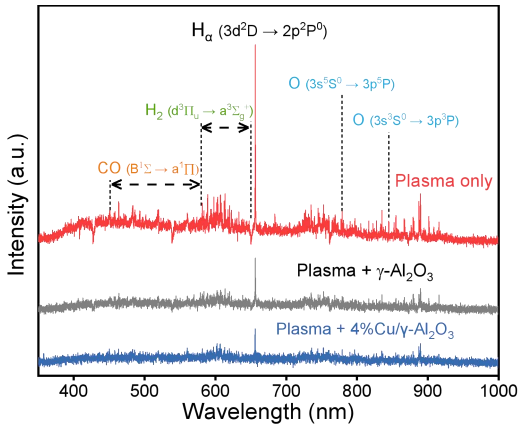

Fig. 3 OES results for different plasma catalysis conditions.

The signal intensity was obviously reduced after packing the support, which may be caused by the shielding effect.[60] Interestingly, the signal intensity was further reduced after packing with Cu/γ-Al_2O_3 catalyst. To verify if this was caused by optical interference from the packed catalysts, we used UV-Vis spectroscopy to study the light absorption properties of the Cu/γ-Al_2O_3 catalyst. We can see from Fig. S4 in SI that the Cu/γ-Al_2O_3 catalyst shows an obvious absorption peak for UV-light (200-400 nm), but a much lower absorption intensity for visible light (400-800 nm). Because all the lines and bands of interest are located in the wavelength range of visible light, it is reasonable to believe that the reduction of OES intensity is caused not only by optical interference from the packed catalysts, but also by the ability of the active sites to adsorb the reactive species. The reactive CO and H species could promote the CH_3OH production via E-R reactions over the catalyst surface (see section 3.6 below). Besides, changes in the relative strength of the peaks in these three OES systems correspond well with the product selectivity in Fig.1(a), where the CO selectivity exceeds 90 % in the plasma-only system, while the CH_3OH selectivity significantly increases when packing the Cu/γ-Al_2O_3 catalyst in the reactor.

According to Fig. S5, the OES intensity decreases with increasing H_2O/CO_2 molar ratio, which is probably caused by the ionization of H_2O. Besides, as could be deduced from Fig. S2, the discharge performance is reduced by adding H_2O, especially the intensity of the filaments. This may indicate that at higher H_2O content, more energy is consumed by ionization of H_2O, and less energy is consumed by CO_2 and H_2. Hence, this process negatively impacts the CH_3OH production, resulting in a higher energy consumption.

3.3 Catalyst characterization. We characterized the Cu/γ-Al_2O_3 catalyst (with 4 wt.% loading) by XRD, XPS, H_2-TPR and HAADF-STEM and present them in Fig.4. More information about the catalysts, i.e., N_2 physisorption data (Table S2) and elementary mapping results (Fig. S6), can be found in Supplementary Materials. Fig. 4(a) shows the XRD results. The diffraction peaks are all attributed to γ-Al_2O_3, and no diffraction peaks related to Cu species are observed for the Cu-based catalysts, indicating that Cu is highly dispersed on γ-Al_2O_3. Fig. 4(b) shows the XPS results. For the fresh sample, two peaks at 934.9 eV and 955.3 eV are observed, and they are attributed to Cu $2p_{3/2}$ and Cu $2p_{1/2}$ of Cu^{2+} species, respectively. In addition, the presence of Cu^{2+} is confirmed by the appearance of oscillating satellite peaks at 943 eV and 963.1 eV.[61] For the reduced samples, the apparent weakening of the signal intensity at 934.9 eV and 955.3 eV, as well as the two satellite peaks, demonstrate the disappearance of Cu^{2+} species, which is caused by H_2 plasma reduction.[62] The peaks of Cu^{2+} species are observed only with low intensity, which is attributed to the fact that the catalyst is susceptible to being oxidized by air (during the transfer of the sample from the plasma reactor to the XPS instrument) to produce CuO species on the sample surface. Even so, two peaks (932.5 eV and 952.3 eV) assigned to Cu^0 species are observed with much higher intensity than those of Cu^{2+} species, which means that Cu^0 species are dominant in the reduced sample. This observation is consistent with the H_2-TPR results (Fig. 4(c), where no distinctive peaks are seen for the reduced catalyst, suggesting that Cu^{m+} are all reduced to Cu^0 at 573 K.

Fig. 4(d-f) show the HAADF-STEM images of the 4 wt.% Cu/γ-Al_2O_3 samples. Clearly, Cu is highly dispersed on the γ-Al_2O_3 support, with particle size in the range of 0.8-2 nm. In our DFT calculations, we consider a Cu_{13} cluster on γ-Al_2O_3, which roughly corresponds to the same particle size as in our experiments. Indeed, it is extremely challenging to synthesize a Cu/γ-Al_2O_3 catalyst with pure Cu_{13} clusters, but the DFT results should be able to provide more insight in the underlying mechanisms, to explain the experimental results.

The spent Cu/γ-Al_2O_3 catalyst after 3 h plasma reaction has been characterized by XRD, H_2-TPR and XPS (Fig. S7), which shows the coexistence of Cu^0, Cu^+ and Cu^{2+} species. Hence, Cu species cannot remain the Cu^0 valence state during the CO_2/H_2 plasma reaction, since O atoms from CO_2 dissociation will oxidize Cu^0 to produce Cu_2O and CuO. On the other hand, H species from H_2 dissociation play the role of reducing agent. Therefore, the CO_2/H_2 plasma reaction contains a dynamic reduction-oxidation process, yielding a dynamic reduction-oxidation of the Cu species (Cu^0, Cu^+ and Cu^{2+}).

In the following sections, we will study the CO_2 hydrogenation to CH_3OH over the Cu_{13}/γ-Al_2O_3 surface by DFT calculations, to obtain more insight in the underlying mechanisms. First we will present the activation of CO_2 over

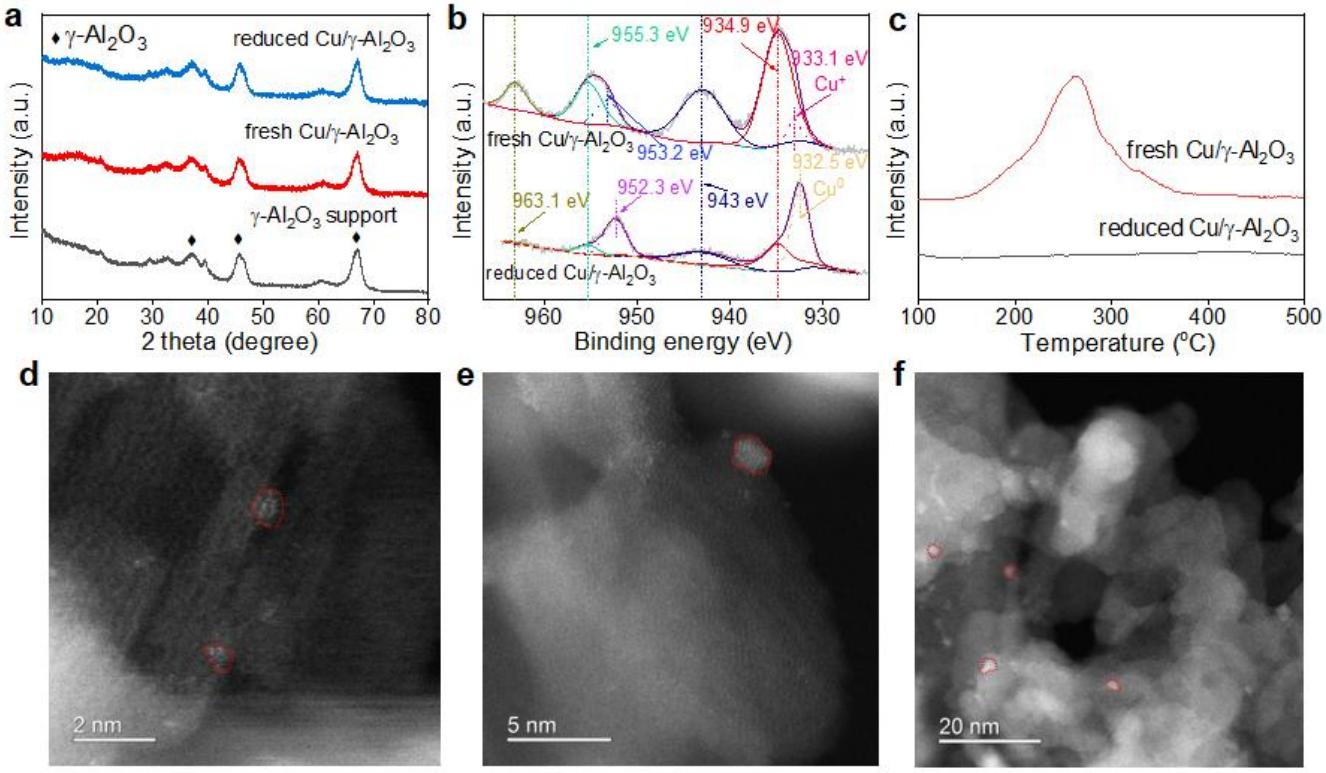

Fig. 4 Characterization of the Cu/γ-Al_2O_3 catalyst: (a) XRD patterns; (b) Cu 2p XPS spectra; (c) H_2-TPR profiles; (d-f) HAADF-STEM images.

the Cu_{13}/γ-Al_2O_3 surface. Next, we will analyze the hydrogenation pathways of CO_2 to CH_3OH and CH_4 via the L-H mechanism. Finally, we will present the E-R reactions caused by the reactive plasma species and analyze the promotion effect of H_2O molecules on CH_3OH desorption.

3.4 Cu_{13} supported on γ-Al_2O_3(110) and CO_2 adsorption site selection. The Cu_{13} icosahedron cluster is a common and stable structure, which has been used to represent Cu nano-cluster structures in previous DFT studies.[49] In this work, the Cu_{13}/γ-Al_2O_3(110) model is chosen to represent Cu clusters supported by a γ-Al_2O_3 slab, as shown in Fig. S9. The Cu_{13} cluster is first optimized in the gas phase and subsequently allowed to adsorb on the γ-Al_2O_3 substrate, with the Cu atoms binding with the surface O and Al atoms. The adsorption energy E_{ad} is -4.35 eV, which is weaker than the adsorption on a typical hydrated γ-Al_2O_3 surface (-6.13 eV).[49] This may be caused by the difference of pre-adsorbed species on the γ-Al_2O_3 surface.

Before the hydrogenation calculation, we first tested the potential adsorption sites on the Cu_{13}/γ-Al_2O_3(110) surface. According to SMC studies, the interface of the metal cluster and the support are most likely to be the active sites.[14,45,63]

Therefore, five typical sites are selected, four of them are interface sites around the Cu_{13} cluster and one site is on the top of the cluster, as shown in Fig. S10. The adsorption energies of two reactants (CO_2 and H_2) and two products (CH_3OH and H_2O) are calculated and are summarized in Table S3. It is clear that site number 3 at the cluster-slab interface is the most stable site for all four molecules (CO_2, H_2, CH_3OH and H_2O). Therefore, the site number 3 is chosen as the active site for further calculations, and the most stable configurations of the four molecules are shown in Fig. S11.

As shown in Fig. S12(a), after the adsorption, the CO_2 molecule at Cu_{13}/γ-Al_2O_3 interface binds with the Cu atoms and with the slab Al atom, with an O-C-O angle bending from 180° to 121.08°. The two C-O bonds are elongated from 1.18 Å to 1.29 Å. According to the Bader charge analysis and the charge density difference in Fig. S12(b), the adsorbed CO_2 molecule gains 1.24 |e|, where the C atom gains 1.64 |e|, and the O1 and O2 atoms lose 0.31 |e| and 0.09 |e|, respectively. The above results indicate that when the CO_2 molecule is adsorbed, the Cu_{13}/γ-Al_2O_3 catalyst acts as an electron donor to transfer electrons to the C atom, while it acts as an electron accept or to take electrons from the O atoms, leading to a weakening of the C-O bonds. In contrast, we found that the adsorption and activation of CO_2 molecules on Cu_{13} cluster surface is a bit weaker. In Fig.S12(c), O-C-O angle bends from 180° to 134.48° and the two C-O bonds stretch from 1.18 Å to 1.28 and 1.22 Å, respectively. This result agrees well with former DFT results[63] and the adsorbed CO_2 coordinated in the metal-support interface becomes more active for further reactions. Among all the calculated sites, the num.3 interface site shows a better effect for CO_2 activation.

In addition, we found that the H_2 adsorbed at the Cu_{13}/γ-Al_2O_3 interface is decomposed to two H* without an obvious barrier, as shown in Fig. S11(b), which agrees with previous DFT results.[31] Moreover, we tested the H_2 decomposition on the Cu_{13} surface and it has a very small barrier of 0.44 eV. Thus, the H_2 decomposition will not be involved in detail in subsequent hydrogenation reactions.

3.5 CH_3OH synthesis at the interface of Cu_{13}/γ-Al_2O_3 via the L-H mechanism. The main reaction pathways for CH_3OH formation and one additional pathway for CH_4 formation are shown in Fig. 5. All the elementary reactions are first calculated via the L-H mechanism. The rate-limiting step of the formate path is HCOOH formation with a barrier of 1.32 eV, which is smaller than the rate-limiting step of the RWGS path, i.e., COOH* formation ('*' means the adsorbed species)

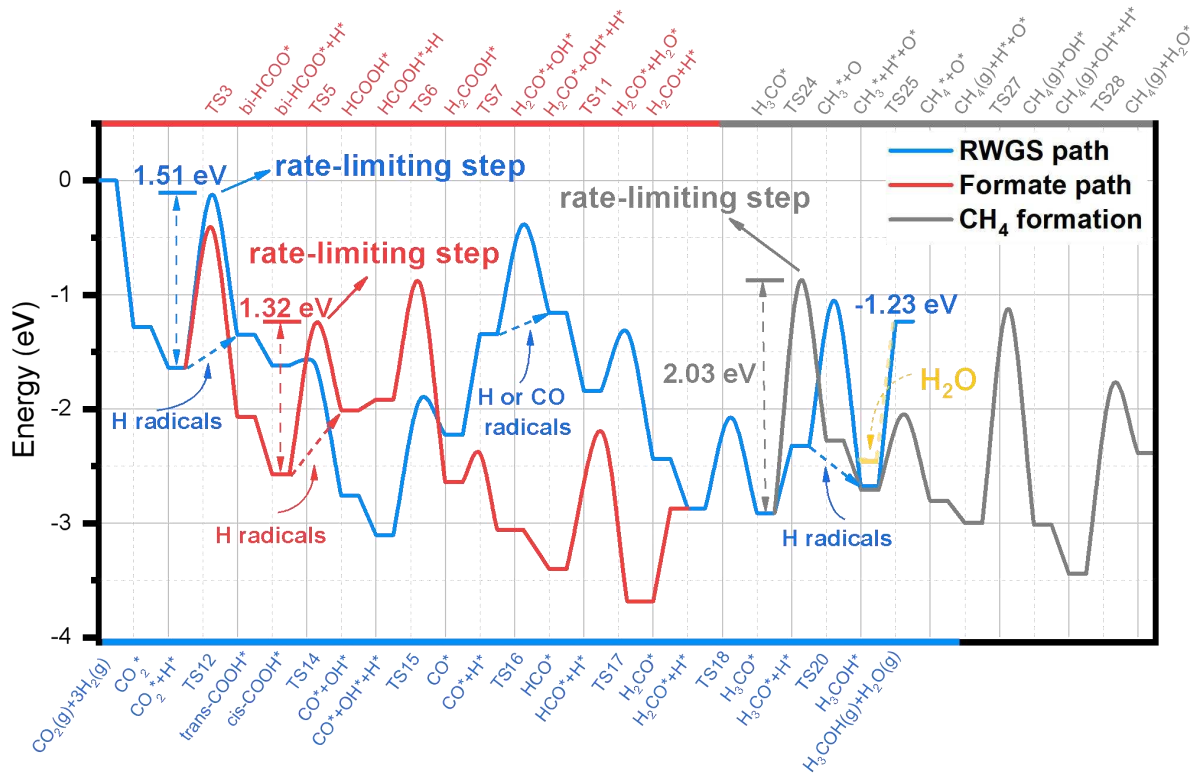

Scheme 1. Reaction pathways of CO_2 hydrogenation to CH_3OH and CH_4. Species adsorbed at active sites are labeled as '*'. To make the figure more readable, H_2 decomposition and H_2O desorption are omitted from the pathways.

with a barrier of 1.51 eV. The results of rate-limiting steps in different paths of Cu-based catalysts similarly appeared in previous studies.[15,32,64] The BE of important intermediates and the reaction barrier and heat of elementary reactions are listed in Table S4 and Table S5, respectively. The intermediates in CH_3OH synthesis can be stably adsorbed at the Cu_{13}/γ-Al_2O_3 interface site, resulting in an energetically lower reaction pathway.

In the formate path, HCOO* is first generated by CO_2 hydrogenation. Subsequently, HCOO* is hydrogenated to formic acid (HCOOH*) with a further hydrogenation of HCOOH* to H_2COOH*. Afterwards, H_2COOH* is decomposed to H_2CO* and OH* with the breaking of the C-OH bond. Further hydrogenation of H_2CO* leads to the formation of CH_3OH via H_2COH* or H_3CO*. In Scheme S1, we compare the energy barrier of three paths from HCOO* to H_2CO*. The HCOOH* path exhibits the lowest barrier of 1.32 eV, while the other two paths via H_2COO* show barriers of 2.11 eV and 1.51 eV, respectively. This indicates that the HCOOH* path is more favored than the two H_2COO* paths over the Cu_{13}/γ-Al_2O_3 surface and a similar distribution of the barriers is also found on Cu(111) surface.[31] Besides, both in our model and on the Cu(111) surface, the BE of HCOOH* (-2.01 eV) is lower than that of H_2COO* (-2.34 eV) which shows a similar catalytic effect of Cu atoms either as a cluster or being a bulk.

Besides, we calculated the CH_3OH formation from H_2CO* hydrogenation via H_2COH* or H_3CO* intermediates, as shown in Scheme S2. These two paths have very similar barriers, i.e., 1.27 eV in the H_2COH path and 1.25 eV in the H_3CO path. The barrier of the H_3CO* path is slightly lower than the H_2COH*path, and its energy curve lies lower than for the H_2COH* path. Besides, the BE of CH_3O* (-4.52 eV) is much larger than that of H_2COH* (-2.83 eV), resulting in a higher stability of CH_3O*. Previous studies have shown that the higher stability and abundance of H_3CO* may counteract the higher activation barrier and make the H_3CO* path dominant.[31,65,66] Therefore, we take the H_3CO* path as the main path and this is summarized in Scheme 1. In this pathway, the elementary steps of HCOO* to HCOOH* and H_3CO* to CH_3OH show the highest reaction barriers, consistent with the result in a Cu/ZnO system, where the Cu-ZnO interface also acts as an active site.[13] This may indicate that the combination of metal-oxide form of Cu-based catalysts provides active sites at the interface over the nanoparticle/slab structure, which shows a multiple catalytic effect on both the activation and the hydrogenation of CO_2.

In the COOH path, the barrier for CO_2 hydrogenation to COOH* is 1.51 eV, which is higher than for the HCOO* formation (1.23 eV), and it makes this reaction become the rate-limiting step for this path. Afterwards, COOH* can easily decompose to CO* and OH* at the Cu_{13}/γ-Al_2O_3 interface without an obvious barrier, which is similar to the results on a single Cu_{29} cluster or on a Cu(111) slab.[32,33] Subsequently, CO* is gradually hydrogenated to H_2CO* via HCO*. As shown in Table S3, the BE of CO* at the interface site is -1.98 eV, corresponding to a chemical adsorption with strong surface interactions. This promotes the further hydrogenation rather than a desorption process.[67] Overall, the RWGS path lays higher than the formate path in energy distribution, which means that the RWGS path is more significant at high temperature. In plasma catalysis, the reactor is maintained at a relatively low temperature (around 400K). Therefore, if not considering the plasma effect, the formate path is likely to be predominant due to its lower rate-limiting step.

Apart from the RWGS path, CO* may also be generated by

CO_2* decomposition. However, one C-O bond-breaking requires 2.08 eV (Table S4), i.e., much higher than the hydrogenation reactions, which indicates that CO_2 direct decomposition to CO is difficult on a Cu_{13}/γ-Al_2O_3 surface.

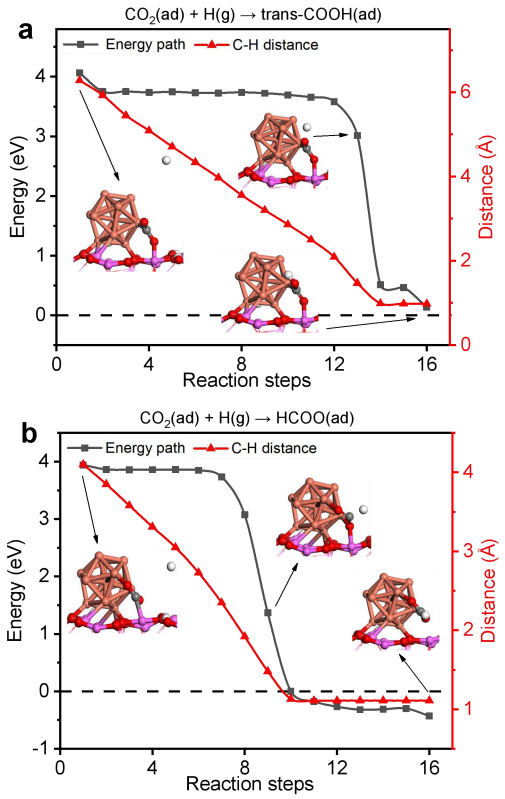

Fig. 5 Formation of COOH and HCOO via the E-R mechanism. (a) COOH; (b) HCOO.

Moreover, we calculated the path of CH_4 formation. This path begins with the decomposition of H_3CO*. As shown in Scheme 1, the cleavage of the C-O bond for H_3CO* species needs to overcome a high barrier (2.03 eV), much higher than in H_3CO* hydrogenation, which is in agreement with a previous DFT study.[15] Although the hydrogenation of CH_3* to CH_4 (g) has a low barrier of 0.66 eV, the following hydrogenation steps for decomposed O* to OH* and further to H_2O* also have high barriers (1.87 eV and 1.64 eV). Therefore, the DFT results indicate that CH_4 formation via the above path has much high barriers than CH_3OH production, which can explain the much lower yield of CH_4 in the experiment.

3.6 Effect of plasma species via the E-R mechanism. Previous studies have demonstrated that plasma species can participate in surface hydrogenation reactions via the E-R mechanism.[68,69] 1D fluid plasma chemistry simulations showed that, in CO_2/H_2 plasma, H and CO are the two most abundant species.[70] Therefore, we considered these two plasma species for studying the plasma effects via the E-R reactions. Along the two reaction paths, the initial step for CO_2 hydrogenation, the rate-limiting steps, and the final CH_3OH formation reaction are calculated with H radicals participating. Besides, the CO molecules are considered to be bonded with H* to form the HCO* species, as an alternative way for the RWGS path. Compared with the L-H reactions, the activation barriers are obviously reduced in the E-R reactions when plasma species are involved. For instance, it can be seen from Fig. 5 that trans-COOH* and HCOO* are formed when CO_2* binds with gas-phase H radicals without a barrier. At the very start, the energy of the whole system is much higher than in the L-H reaction, which is attributed to the reactive H species generated in the plasma.[60] The gas-phase H atom moves to the Cu_{13}/γ-Al_2O_3 interface and binds with CO_2, which leads to a sharp decrease of the system energy when the O-H distance approaches about 2 Å. This barrierless E-R reaction indicates that the plasma-generated H atoms may accelerate the CO_2 hydrogenation by changing the reaction mechanism. Similar results appear in the formation of HCOOH and CH_3OH. In Fig. S13, HCOOH* is generated from HCOO* hydrogenation with H radicals, with a barrier reduced from 1.32 eV to 0.17 eV, which indicates that the HCOOH formation may no longer be the rate-limiting step in the formate path. In Fig. S14, H_3CO* hydrogenation with H radicals to form CH_3OH has a barrier of 0.15 eV, much lower than the barrier of the L-H reaction, i.e., 1.25 eV.

Besides, HCO* can be generated when the gas-phase CO species bind with H*, or the gas-phase H atoms bind with CO*, via two barrierless E-R reactions, as shown in Fig. S15 and Fig. S16. These two barrierless reactions prove that the CO and H species generated in the plasma are highly reactive and can facilitate the HCO* formation. It is known that HCO is an important intermediate and its stability on the catalyst surface is also identified as a key factor affecting the whole RWGS path.[33] In addition, the binding strength of key intermediates over metal-oxide catalysts may also determine the reaction types and selectivity of CO_2 hydrogenation. In our calculations, HCO* can be generated in both L-H and E-R reactions, and can be stably adsorbed at the interface site.[67] Besides, our OES results prove that CO and H are abundantly produced in the plasma and can be effectively adsorbed on the catalyst surface, to take part in further reactions. Therefore, in plasma catalysis, the RWGS path may become more significant, as the HCO* species generated via the E-R reactions may provide an alternative way for CH_3OH* formation with lower barriers.

In thermal catalysis, intermediates like HCOO may also be produced via the E-R mechanism. Compared to reactions involving the radicals, the reduction in activation barriers is limited and the barriers cannot be eliminated.[71,72] Overall, the plasma effect can influence the CO_2 hydrogenation via the E-R reactions. The participation of plasma species significantly reduces or even eliminates the energy barriers and in the meantime provide key intermediates for the elementary reactions, resulting in a high CH_3OH selectivity and yield at such low temperature (ct. 60 °C) and at atmospheric pressure.

3.7 Role of H_2O in CH_3OH desorption. As mentioned above, the plasma effect can accelerate the hydrogenation process, but it may not necessarily promote CH_3OH desorption. In previous studies, the H_2O molecule is demonstrated to be an effective promoter for CH_3OH* generation and desorption.[32,73,74] Therefore, we calculated the CH_3OH E_{ad} and configurations in the presence and absence of pre-adsorbed H_2O, as shown in Table 1. and Fig. S17, respectively. In the absence of H_2O, CH_3OH* is stably adsorbed at the Cu_{13}/γ-Al_2O_3 interface with an adsorption energy E_{ad} of -1.45 eV (Fig. S11a). When H_2O is pre-adsorbed, the E_{ad} of CH_3OH* is reduced. In Fig. S17d, one H_2O molecule can be co-adsorbed with CH_3OH at the Cu_{13}/γ-Al_2O_3 site and E_{ad} of CH_3OH* is decreased to -1.23 eV. In Fig. S17f, CH_3OH adsorbed at the nearby γ-Al_2O_3 slab has an E_{ad} of -1.25 eV, which is more stable than at the interface site. When two H_2O molecules are pre-adsorbed at the interface site, the E_{ad} of CH_3OH* is reduced to -1.17 eV (Fig. S17g), which is also weaker than at the γ-Al_2O_3 slab site (-1.28eV, Fig. S17i). This indicates that the H_2O generated from reactions or added in the initial gas mixture may be pre-adsorbed at the catalyst

Table 1. Comparison of E_{ad} of CH_3OH over Cu_{13}/γ-Al_2O_3 surface at different H_2O pre-adsorption conditions.

H_2O number	H_2O adsorption site	CH_3OH adsorption site	CH_3OH adsorption energy (eV)
0	——	Cu_{13}/γ-Al_2O_3 interface	-1.45
0	——	Cu_{13} cluster	-0.84
0	——	γ-Al_2O_3 slab	-1.34
1	Cu_{13}/γ-Al_2O_3 interface	Cu_{13}/γ-Al_2O_3 interface	-1.23
1	Cu_{13}/γ-Al_2O_3 interface	Cu_{13} cluster	-0.80
1	$Cu_{13}\gamma$-/Al_2O_3 interface	γ-Al_2O_3 slab	-1.25
2	$Cu_{13}\gamma$-/Al_2O_3 interface	Cu_{13}/γ-Al_2O_3 interface	-1.17
2	Cu_{13}/γ-Al_2O_3 interface	Cu_{13} cluster	-0.74
2	Cu_{13}/γ-Al_2O_3 interface	γ-Al_2O_3 slab	-1.28

surface and reduce the CH_3OH adsorption energy at its most stable site, which in a way promotes the desorption of CH_3OH. This agrees with our experimental results that H_2O addition increases the CH_3OH selectivity. However, it should also be noted that the excess addition of H_2O could inhibit the CH_3OH production as shown in Fig. 2(b) and this also attributes to the competitive adsorption of the active sites, which negatively impact the hydrogenation of CO_2 and the adsorption of important intermediates.[75,73]

3.8 Final consideration. Overall, the Cu/γ-Al_2O_3 catalyst shows a good performance in plasma-catalytic CO_2 hydrogenation to CH_3OH. Our DFT simulations reveal that this is attributed to the high catalytic activity of the Cu atoms and the metal-support interaction. The interface site on Cu_{13}/γ-Al_2O_3 is considered to be bifunctional. Firstly, it can effectively activate the CO_2 molecules. In addition, the intermediates in the CH_3OH synthesis process can be strongly adsorbed at this site, avoiding their desorption. CH_3OH can be generated through both RWGS and formate paths, while the CH_4 formation path is reduced due to its high activation barriers.

A thermal catalysis study showed that a 2-4 mm Cu cluster supported on γ-Al_2O_3 can catalyze the hydrogenation of CO_2 to CH_3OH, accompanied by the generation of CO and dimethyl ether (DME).[62] Their DFT results also prove that the interface between the Cu cluster and the Al_2O_3 slab is the active site. DME and CO are produced by further dehydrogenation of CH_3OH and decomposition of surface species, respectively. Although we applied a similar Cu/γ-Al_2O_3 catalyst in plasma catalysis, DME did not show up in our experiments. This could be attributed to the synergistic effect between plasma and catalyst, where the plasma species can accumulate on the catalyst surface and promote the CH_3OH desorption.[70] Besides, the adsorption of CH_3OH in our system is relatively weak due to the H_2O competitive adsorption, so that desorption is easier than further dehydrogenation. Moreover, according to the analysis by Lam et al., competitive RWGS reactions could negatively impact the CH_3OH synthesis to reduce its yield and selectivity.[62] However, in plasma catalysis, the CO species generated in the plasma or at the catalyst surface may further participate in the surface reactions via the E-R mechanism, and promote the selectivity towards CH_3OH.[77]

In addition, complicated interactions can take place between plasma and catalyst. Due to polarization effects, the Cu/γ-Al_2O_3 packing can effectively enhance the electric field inside the plasma, which leads to a more intense plasma and a higher density of plasma species.[78,79] Hence, these plasma species can participate in the CO_2 hydrogenation process via E-R reactions, to reduce the reaction barriers and promote the generation of key intermediates in the catalytic reactions. Therefore, the plasma species can change the elementary reactions and tune the reaction pathways.

Furthermore, the plasma effects are not limited to E-R reactions. The electric field enhancement, as well as surface charging, may enhance the adsorption of CO_2 and promote its activation over the catalyst surface.[80,81] In addition, the pre-adsorbed species on the catalyst surface or vibrational excited species in plasma catalysis can influence the surface reactions and hydrogenation process.[45,82] These effects are not yet accounted for in our DFT calculations, but may also be important to comprehensively understand the complete picture of plasma catalysis. Future studies should therefore include more detailed DFT calculations, as well as in-situ experiments.

4. CONCLUSIONS

We studied plasma-catalytic CO_2 hydrogenation to CH_3OH over a γ-Al_2O_3 supported Cu cluster catalyst, both experimentally and by DFT calculations to reveal the underlying mechanisms, with special focus on the role of plasma species via E-R mechanisms. The presence of plasma allowed us to achieve a CO_2 conversion of 10% with a maximum CH_3OH selectivity of 65%, while no CO_2 conversion took place without plasma at these conditions (room temperature and atmosphere pressure). Furthermore, the undesired CH_4 yield was reduced to below 2%. In addition, the energy efficiency was improved by more than a factor 20 when combining the plasma and the Cu/γ-Al_2O_3 catalyst, as compared to plasma-only, indicates the key role of the active metal (Cu cluster) for efficiently producing CH_3OH. Our DFT results revealed that the interface site of Cu_{13}/γ-Al_2O_3 hosts multiple active sites for both the CO_2 activation and the hydrogenation. The reactive species generated in the plasma region could shift the barriers from the surface to the gas phase, thus reducing or eliminating the reaction barrier via the E-R mechanism, which makes the reaction take place at atmospheric conditions. Besides, H_2O competitive adsorption on the catalyst surface could promote the desorption of CH_3OH, thus increasing its selectivity. This study gives new insights into plasma-catalytic CO_2 hydrogenation to CH_3OH, and may also have potential applications in other (plasma-)catalytic research, especially for SMC catalysts.

AUTHOR INFORMATION

Corresponding Author

Yanhui Yi − *State Key Laboratory of Fine Chemicals, School of Chemical Engineering, Dalian University of Technology, Dalian 116024, P. R. China; Research group PLASMANT, Department of Chemistry, University of Antwerp, Universiteitsplein 1, BE-2610 Wilrijk-Antwerp, Belgium;*
Email: yiyanhui@dlut.edu.cn

Xiaoxing Zhang − *School of Electrical and Electronic Engineering, Hubei University of Technology, Wuhan, 430068, China;*
Email: xiaoxingzhang@outlook.com

Authors

Zhaolun Cui − *School of Electric Power Engineering, South China University of Technology, Guangzhou 510630, China; Research group PLASMANT, Department of Chemistry, University of Antwerp, Universiteitsplein 1, BE-2610 Wilrijk-Antwerp, Belgium*

Shengyan Meng − *State Key Laboratory of Fine Chemicals, School of Chemical Engineering, Dalian University of Technology, Dalian 116024, P. R. China*

Amin Jafarzadeh − *Research group PLASMANT, Department of Chemistry, University of Antwerp, Universiteitsplein 1, BE-2610 Wilrijk-Antwerp, Belgium*

Shangkun Li − *Research group PLASMANT, Department of Chemistry, University of Antwerp, Universiteitsplein 1, BE-2610 Wilrijk-Antwerp, Belgium*

Erik C Neyts − *Research group PLASMANT, Department of Chemistry, University of Antwerp, Universiteitsplein 1, BE-2610 Wilrijk-Antwerp, Belgium*

Yanpeng Hao − *School of Electric Power Engineering, South China University of Technology, Guangzhou 510630, China*

Licheng Li − *School of Electric Power Engineering, South China University of Technology, Guangzhou 510630, China*

Xinkui Wang − *State Key Laboratory of Fine Chemicals, School of Chemical Engineering, Dalian University of Technology, Dalian 116024, P. R. China*

Annemie Bogaerts − *Research group PLASMANT, Department of Chemistry, University of Antwerp, Universiteitsplein 1, BE-2610 Wilrijk-Antwerp, Belgium*

Author Contributions

The manuscript was written through contributions of all authors. All authors have given approval to the final version of the manuscript.

Notes

The authors declare no competing financial interest.

ASSOCIATED CONTENT

Supporting Information

The Supporting Information is available free of charge at https://pubs.acs.org
It contains more experimental details, choice of the supported cluster model and computational details.

ACKNOWLEDGMENTS

This research was funded by the National Natural Science Foundation of China [21503032, 21978032], the European Research Council (ERC) under the European Union's Horizon 2020 research and innovation programme (ERC Synergy Grant 810182 SCOPE). The computational resources and services used in this work were provided by the HPC core facility CalcUA of the Universiteit Antwerpen, and VSC (Flemish Supercomputer Center), funded by the Research Foundation - Flanders (FWO) and the Flemish Government.

REFERENCES

(1) Bao, J.; Yang, G.; Yoneyama, Y.; Tsubaki, N., Significant Advances in C1 Catalysis: Highly Efficient Catalysts and Catalytic Reactions. *ACS Catal.* **2019**, 9 (4), 3026-3053.
(2) Snoeckx, R.; Bogaerts, A., Plasma technology-a novel solution for CO_2 conversion? *Chem. Soc. Rev.* **2017**, 46 (19), 5805-5863.
(3) Jiang, X.; Nie, X.; Guo, X.; Song, C.; Chen, J. G., Recent Advances in Carbon Dioxide Hydrogenation to Methanol via Heterogeneous Catalysis. *Chem. Rev.* **2020**, 120 (15), 7984-8034.
(4) Zhong, J.; Yang, X.; Wu, Z.; Liang, B.; Huang, Y.; Zhang, T., State of the art and perspectives in heterogeneous catalysis of CO_2 hydrogenation to methanol. *Chem. Soc. Rev.* **2020**, 49 (5), 1385-1413.
(5) Behrens, M.; Studt, F.; Kasatkin, I.; Kuehl, S.; Haevecker, M.; Abild-Pedersen, F.; Zander, S.; Girgsdies, F.; Kurr, P.; Kniep, B.-L.; Tovar, M.; Fischer, R. W.; Norskov, J. K.; Schloegl, R., The Active Site of Methanol Synthesis over $Cu/ZnO/Al_2O_3$ Industrial Catalysts. *Science* **2012**, 336 (6083), 893-897.
(6) Graciani, J.; Mudiyanselage, K.; Xu, F.; Baber, A. E.; Evans, J.; Senanayake, S. D.; Stacchiola, D. J.; Liu, P.; Hrbek, J.; Fernandez Sanz, J.; Rodriguez, J. A., Highly active copper-ceria and copper-ceria-titania catalysts for methanol synthesis from CO_2. *Science* **2014**, 345 (6196), 546-550.
(7) Kim, J.; Sarrna, B. B.; Andres, E.; Pfander, N.; Concepcion, P.; Prieto, G., Surface Lewis Acidity of Periphery Oxide Species as a General Kinetic Descriptor for CO_2 Hydrogenation to Methanol on Supported Copper Nanoparticles. *ACS Catal.* **2019**, 9 (11), 10409-10417.
(8) Chen, S.; Zhang, J.; Song, F.; Zhang, Q.; Yang, G.; Zhang, M.; Wang, X.; Xie, H.; Tan, Y., Induced high selectivity methanol formation during CO_2 hydrogenation over a $CuBr_2$-modified CuZnZr catalyst. *J. Catal.* **2020**, 389, 47-59.
(9) Wu, C.; Lin, L.; Liu, J.; Zhang, J.; Zhang, F.; Zhou, T.; Rui, N.; Yao, S.; Deng, Y.; Yang, F.; Xu, W.; Luo, J.; Zhao, Y.; Yan, B.; Wen, X.-D.; Rodriguez, J. A.; Ma, D., Inverse ZrO_2/Cu as a highly efficient methanol synthesis catalyst from CO_2 hydrogenation. *Nat. Commun.* **2020**, 11 (1), 5767-5776.
(10) Tada, S.; Otsuka, F.; Fujiwara, K.; Moularas, C.; Deligiannakis, Y.; Kinoshita, Y.; Uchida, S.; Honma, T.; Nishijima, M.; Kikuchi, R., Development of CO_2-to-Methanol Hydrogenation Catalyst by Focusing on the Coordination Structure of the Cu Species in Spinel-Type Oxide $Mg_{1-x}Cu_xAl_2O_4$. *ACS Catal.* **2020**, 10 (24), 15186-15194.
(11) Zabilskiy, M.; Sushkevich, V. L.; Palagin, D.; Newton, M. A.; Krumeich, F.; van Bokhoven, J. A., The unique interplay between copper and zinc during catalytic carbon dioxide hydrogenation to methanol. *Nat. Commun.* **2020**, 11 (1), 2409.
(12) Cui, X.; Yan, W.; Yang, H.; Shi, Y.; Xue, Y.; Zhang, H.; Niu, Y.; Fan, W.; Deng, T., Preserving the Active Cu-ZnO Interface for Selective Hydrogenation of CO_2 to Dimethyl Ether and Methanol. *ACS Sustain. Chem. Eng.* **2021**, 9 (7), 2661-2672.
(13) Kattel, S.; Ramirez, P. J.; Chen, J. G.; Rodriguez, J. A.; Liu, P., CATALYSIS Active sites for CO_2 hydrogenation to methanol on Cu/ZnO catalysts. *Science* **2017**, 355 (6331), 1296.
(14) Dong, C.; Li, Y.; Cheng, D.; Zhang, M.; Liu, J.; Wang, Y.-G.; Xiao, D.; Ma, D., Supported Metal Clusters: Fabrication and Application in Heterogeneous Catalysis. *ACS Catal.* **2020**, 10 (19), 11011-11045.
(15) Liu, C.; Yang, B.; Tyo, E.; Seifert, S.; DeBartolo, J.; von Issendorff, B.; Zapol, P.; Vajda, S.; Curtiss, L. A., Carbon Dioxide Conversion to Methanol over Size-Selected Cu_4 Clusters at Low Pressures. *J. Am. Chem. Soc.* **2015**, 137 (27), 8676-8679.
(16) Wang, L.; Yi, Y.; Guo, H.; Tu, X., Atmospheric Pressure and Room Temperature Synthesis of Methanol through Plasma-Catalytic Hydrogenation of CO_2. *ACS Catal.* **2018**, 8 (1), 90-100.
(17) Wang, Z.; Zhang, Y.; Neyts, E. C.; Cao, X.; Zhang, X.; Jang, B.

W. L.; Liu, C.-j., Catalyst Preparation with Plasmas: How Does It Work? *ACS Catal.* **2018**, 8 (3), 2093-2110.
(18) Neyts, E. C.; Ostrikov, K.; Sunkara, M. K.; Bogaerts, A., Plasma Catalysis: Synergistic Effects at the Nanoscale. *Chem. Rev.* **2015**, 115 (24), 13408-13446.
(19) Engelmann, Y.; van 't Veer, K.; Gorbanev, Y.; , Neyts, E. C.; Schneider, W. F.; Bogaerts, A., Plasma Catalysis for Ammonia Synthesis: A Microkinetic Modeling Study on the Contributions of Eley–Rideal Reactions. ACS Sustain. *Chem. Eng.* **2021**, 9 (39) 13151-13163.
(20) Iliuta, I.; Larachi, F., Enhanced Methanol Synthesis Process via an Integrated Process Involving CO_2 Hydrogenation under Plasma Conditions. *Ind. Eng. Chem. Res.* **2020**, 59 (15), 6815-6827.
(21) Wang, L.; Yi, Y.; Wu, C.; Guo, H.; Tu, X., One-Step Reforming of CO_2 and CH_4 into High-Value Liquid Chemicals and Fuels at Room Temperature by Plasma-Driven Catalysis. *Angew. Chem., Int. Ed.* **2017**, 56 (44), 13679-13683.
(22) Wang, X.; Gao, Y.; Zhang, S.; Sun, H.; Li, J.; Shao, T., Nanosecond pulsed plasma assisted dry reforming of CH_4: The effect of plasma operating parameters. *Appl. Energy* **2019**, 243, 132-144.
(23) Chen, H.; Goodarzi, F.; Mu, Y.; Chansai, S.; Mielby, J. J.; Mao, B.; Sooknoi, T.; Hardacre, C.; Kegnaes, S.; Fan, X., Effect of metal dispersion and support structure of Ni/silicalite-1 catalysts on non-thermal plasma (NTP) activated CO_2 hydrogenation. *Appl. Catal., B* **2020**, 272.
(24) Ronda-Lloret, M.; Wang, Y.; Oulego, P.; Rothenberg, G.; Tu, X.; Shiju, N. R., CO_2 Hydrogenation at Atmospheric Pressure and Low Temperature Using Plasma-Enhanced Catalysis over Supported Cobalt Oxide Catalysts. *ACS Sustain. Chem. Eng.* **2020**, 8 (47), 17397-17407.
(25) Xu, S.; Chansai, S.; Shao, Y.; Xu, S.; Wang, Y.-c.; Haigh, S.; Mu, Y.; Jiao, Y.; Stere, C. E.; Chen, H.; Fan, X.; Hardacre, C., Mechanistic study of non-thermal plasma assisted CO_2 hydrogenation over Ru supported on MgAl layered double hydroxide. *Appl. Catal., B* **2020**, 268.
(26) Bogaerts, A.; Tu, X.; Whitehead, J. C.; Centi, G.; Lefferts, L.; Guaitella, O.; Azzolina-Jury, F.; Kim, H.-H.; Murphy, A. B.; Schneider, W. F.; Nozaki, T.; Hicks, J. C.; Rousseau, A.; Thevenet, F.; Khacef, A.; Carreon, M., The 2020 plasma catalysis roadmap. *J. Phys. D* **2020**, 53 (44), 443001-443052.
(27) Michiels, R.; Engelmann, Y.; Bogaerts, A., Plasma Catalysis for CO_2 Hydrogenation: Unlocking New Pathways toward CH_3OH. *J. Phys. Chem. C* **2020**, 124 (47), 25859-25872.
(28) Mu, Y.; Xu, S.; Shao, Y.; Chen, H.; Hardacre, C.; Fan, X., Kinetic Study of Nonthermal Plasma Activated Catalytic CO_2 Hydrogenation over Ni Supported on Silica Catalyst. *Ind. Eng. Chem. Res.* **2020**, 59 (20), 9478-9487.
(29) Ye, J.; Liu, C.-j.; Mei, D.; Ge, Q., Methanol synthesis from CO_2 hydrogenation over a Pd_4/In_2O_3 model catalyst: A combined DFT and kinetic study. *J. Catal.* **2014**, 317, 44-53.
(30) Dang, S.; Qin, B.; Yang, Y.; Wang, H.; Cai, J.; Han, Y.; Li, S.; Gao, P.; Sun, Y., Rationally designed indium oxide catalysts for CO_2 hydrogenation to methanol with high activity and selectivity. *Sci. Adv.* **2020**, 6 (25), eaaz2060.
(31) Grabow, L. C.; Mavrikakis, M., Mechanism of Methanol Synthesis on Cu through CO_2 and CO Hydrogenation. *ACS Catal.* **2011**, 1 (4), 365-384.
(32) Studt, F.; Behrens, M.; Kunkes, E. L.; Thomas, N.; Zander, S.; Tarasov, A.; Schumann, J.; Frei, E.; Varley, J. B.; Abild-Pedersen, F.; Norskov, J. K.; Schloegl, R., The Mechanism of CO and CO_2 Hydrogenation to Methanol over Cu-Based Catalysts. *Chemcatchem* **2015**, 7 (7), 1105-1111.
(33) Zhao, Y-F.; Yang, Y.; Mims, C.; Peden, C. H. F.; Li, J.; Mei, D., Insight into methanol synthesis from CO_2 hydrogenation on Cu(111): Complex reaction network and the effects of H_2O. *J. Catal.* **2011**, 281 (2), 199-211.
(34) Yang, Y.; Evans, J.; Rodriguez, J. A.; White, M. G.; Liu, P., Fundamental studies of methanol synthesis from CO_2 hydrogenation on Cu(111), Cu clusters, and Cu/ZnO (0001). *Phys. Chem. Chem. Phys.* **2010**, 12 (33), 9909-9917.
(35) Hutter, J.; Iannuzzi, M.; Schiffmann, F.; VandeVondele, J., CP2K: atomistic simulations of condensed matter systems. *Wires. Comput. Mol. Sci.* **2014**, 4 (1), 15-25.
(36) VandeVondele, J.; Krack, M.; Mohamed, F.; Parrinello, M.; Chassaing, T.; Hutter, J., QUICKSTEP: Fast and accurate density functional calculations using a mixed Gaussian and plane waves approach. *Comput Phys Commun* **2005**, 167 (2), 103-128.
(37) VandeVondele, J.; Hutter, J., Gaussian basis sets for accurate calculations on molecular systems in gas and condensed phases. *J. Chem. Phys.* **2007**, 127 (11), 114105.
(38) Goedecker, S.; Teter, M.; Hutter, J., Separable dual-space Gaussian pseudopotentials. *Phys. Rev. B* **1996**, 54 (3), 1703-1710.
(39) Krack, M., Pseudopotentials for H to Kr optimized for gradient-corrected exchange-correlation functionals. *Thero. Chem. Acc.* **2005**, 114 (1-3), 145-152.
(40) Perdew, J. P.; Burke, K.; Ernzerhof, M., Generalized gradient approximation made simple. *Phys. Rev. Lett.* **1996**, 77 (18), 3865-3868.
(41) Grimme, S.; Antony, J.; Ehrlich, S.; Krieg, H., A consistent and accurate ab initio parametrization of density functional dispersion correction (DFT-D) for the 94 elements H-Pu. *J. Chem. Phys.* **2010**, 132 (15), 154104.
(42) Head, J. D.; Zerner, M. C., A Broyden—Fletcher—Goldfarb—Shanno optimization procedure for molecular geometries. *Chem. Phys. Lett.* **1985**, 122 (3), 264-270.
(43) Henkelman, G.; Arnaldsson, A.; Jonsson, H., A fast and robust algorithm for Bader decomposition of charge density. *Comput. Mater. Sci.* **2006**, 36 (3), 354-360.
(44) Henkelman, G.; Uberuaga, B. P.; Jonsson, H., A climbing image nudged elastic band method for finding saddle points and minimum energy paths. *J. Chem. Phys.* **2000**, 113 (22), 9901-9904.
(45) Digne, M.; Sautet, P.; Raybaud, P.; Euzen, P.; Toulhoat, H., Use of DFT to achieve a rational understanding of acid-basic properties of γ-alumina surfaces. *J. Catal.* **2004**, 226 (1), 54-68.
(46) Silaghi, M-C.; Comas-Vives, A.; Coperet, C., CO_2 Activation on $Ni/\gamma\text{-}Al_2O_3$ Catalysts by First-Principles Calculations: From Ideal Surfaces to Supported Nanoparticles. *ACS Catal.* **2016**, 6 (7), 4501-4505.
(47) Wischert, R.; Laurent, P.; Coperet, C.; Delbecq, F.; Sautet, P., γ-Alumina: The Essential and Unexpected Role of Water for the Structure, Stability, and Reactivity of "Defect" Sites. *J. Am. Chem. Soc.* **2012**, 134 (35), 14430-14449.
(48) Shirazi, M.; Neyts, E. C.; Bogaerts, A., DFT study of Ni-catalyzed plasma dry reforming of methane. *Appl. Catal., B* **2017**, 205, 605-614.
(49) Bal, K. M.; Huygh, S.; Bogaerts, A.; Neyts, E. C., Effect of plasma-induced surface charging on catalytic processes: application to CO_2 activation. *Plasma Sources Sci. Technol.* **2018**, 27 (2), 024001.
(50) Gutterød, E. S.; Pulumati, S. H.; Kaur, G.; Lazzarini, A.; Solemsli, B. G.; Gunnaes, A. E.; Ahoba-Sam, C.; Kalyva, M. E.; Sannes, J. A.; Svelle, S.; Skulason, E.; Nova, A.; Olsbye, U., Influence of Defects and H_2O on the Hydrogenation of CO_2 to Methanol over Pt Nanoparticles in UiO-67 Metal-Organic Framework. *J. Am. Chem. Soc.* **2020**, 142 (40), 17105-17118.
(51) Wang, Y.; Gao, W.; Li, K.; Zheng, Y.; Xie, Z.; Na, W.; Chen, J. G.; Wang, H., Strong Evidence of the Role of H_2O in Affecting Methanol Selectivity from CO_2 Hydrogenation over $Cu\text{-}ZnO\text{-}ZrO_2$. *Chem* **2020**, 6 (2), 419-430.
(52) Jiang, X.; Nie, X.; Gong, Y.; Moran, C. M.; Wang, J.; Zhu, J.; Chang, H.; Guo, X.; Walton, K. S.; Song, C., A combined experimental and DFT study of H_2O effect on In_2O_3/ZrO_2 catalyst for CO_2 hydrogenation to methanol. *J. Catal.* **2020**, 383, 283-296.
(53) Gorbanev, Y.; Vervloessem, E.; Nikiforov, A.; Bogaerts, A., Nitrogen Fixation with Water Vapor by Nonequilibrium Plasma: toward Sustainable Ammonia Production. *ACS Sustain. Chem. Eng.* **2020**, 8 (7), 2996-3004.
(54) Snoeckx, R.; Ozkan, A.; Reniers, F.; Bogaerts, A., The Quest for Value-Added Products from Carbon Dioxide and Water in a Dielectric Barrier Discharge: A Chemical Kinetics Study. *ChemSusChem* **2017**, 10 (2), 409-424.
(55) Zhao, B.; Liu, Y.; Zhu, Z.; Guo, H.; Ma, X., Highly selective conversion of CO_2 into ethanol on $Cu/ZnO/Al_2O_3$ catalyst with the assistance of plasma. *J. CO_2 Util.* **2018**, 24, 34-39.
(56) Zambrano, G.; Riascos, H.; Prieto, P.; Restrepo, E.; Devia, A.; Rincon, C., Optical emission spectroscopy study of r.f. magnetron sputtering discharge used for multilayers thin film deposition. *Surf.*

Coat. Technol. **2003**, 172 (2-3), 144-149.
(57) Kholodkov, A. V.; Golant, K. M.; Nikolin, I. V., Nano-scale compositional lamination of doped silica glass deposited in surface discharge plasma of SPCVD technology. *Microelectron Eng.* **2003**, 69 (2-4), 365-372.
(58) Czerwiec, T.; Gavillet, J.; Belmonte, T.; Michel, H.; Ricard, A., Determination of O atom density in Ar-O_2, and Ar-O_2-H_2 flowing microwave discharges. *Surf. Coat. Technol.* **1998**, 98 (1-3), 1411-1415.
(59) Granier, A.; Vervloet, M.; Aumaille, K.; Vallee, C., Optical emission spectra of TEOS and HMDSO derived plasmas used for thin film deposition. *Plasma Sources Sci Technol* **2003**, 12 (1), 89-96.
(60) Yi, Y.; Wang, X.; Jafarzadeh, A.; Wang, L.; Liu, P.; He, B.; Yan, J.; Zhang, R.; Zhang, H.; Liu, X.; Guo, H.; Neyts, E. C.; Bogaerts, A., Plasma-Catalytic Ammonia Reforming of Methane over Cu-Based Catalysts for the Production of HCN and H_2 at Reduced Temperature. *ACS Catal.* **2021**, 11 (3), 1765-1773.
(61) Cai, F.; Zhu, W.; Xiao, G., Promoting effect of zirconium oxide on Cu-Al_2O_3 catalyst for the hydrogenolysis of glycerol to 1, 2-propanediol. *Catal. Sci. Technol.* **2016**, 6 (13), 4889-4900.
(62) Yoshida, H.; Hirakawa, T.; Oyama, H.; Nakashima, R.; Hinokuma, S.; Machida, M., Effect of Thermal Aging on Local Structure and Three-Way Catalysis of Cu/Al_2O_3. *J. Phys. Chem. C* **2019**, 123 (16), 10469-10476.
(63) Lam, E.; Jose Corral-Perez, J.; Larmier, K.; Noh, G.; Wolf, P.; Comas-Vives, A.; Urakawa, A.; Coperet, C., CO_2 Hydrogenation on Cu/Al_2O_3: Role of Metal/Support Interface in Driving Activity and Selectivity of a Bifunctional Catalyst. *Angew. Chem., Int. Ed.* **2019**, 58 (39), 13989-13996.
(64) Sun, Q.; Liu, C. W.; Pan, W.; Zhu, Q. M.; Deng, J. F., In situ IR studies on the mechanism of methanol synthesis over an ultrafine Cu/ZnO/Al_2O_3 catalyst. *Appl. Catal., A* **1998**, 171 (2), 301-308.
(65) Edwards, J. F.; Schrader, G. L., In situ Fourier transform infrared study of methanol synthesis on mixed metal oxide catalysts. *J. Catal.* **1985**, 94 (1), 175-186.
(66) Clarke, D. B.; Bell, An infrared study of methanol synthesis from CO_2 on clean and potassium-promoted Cu/SiO_2. *J. Catal.* **1995**, 154 (2), 314-328.
(67) Kattel, S.; Liu, P.; Chen, J. G., Tuning Selectivity of CO_2 Hydrogenation Reactions at the Metal/Oxide Interface. *J. Am. Chem. Soc.* **2017**, 139 (29), 9739-9754.
(68) Azzolina-Jury, F.; Thibault-Starzyk, F., Mechanism of Low Pressure Plasma-Assisted CO_2 Hydrogenation Over Ni-USY by Microsecond Time-resolved FTIR Spectroscopy. *Top. Catal.* **2017**, 60 (19-20), 1709-1721.
(69) Xu, S.; Chansai, S.; Xu, S.; Stere, C. E.; Jiao, Y.; Yang, S.; Hardacre, C.; Fan, X., CO Poisoning of Ru Catalysts in CO_2 Hydrogenation under Thermal and Plasma Conditions: A Combined Kinetic and Diffuse Reflectance Infrared Fourier Transform Spectroscopy-Mass Spectrometry Study. *ACS Catal.* **2020**, 10 (21), 12828-12840.
(70) De Bie, C.; van Dijk, J.; Bogaerts, A., CO_2 Hydrogenation in a Dielectric Barrier Discharge Plasma Revealed. *J. Phys. Chem. C* **2016**, 120 (44), 25210-25224.
(71) Wang, G. C.; Morikawa, Y.; Matsumoto, T.; Nakamura, J., Why is formate synthesis insensitive to copper surface structures? *J. Phys. Chem. B* **2006**, 110 (1), 9-11.
(72) Mei, D.; Xu, L.; Henkelman, G., Dimer saddle point searches to determine the reactivity of formate on Cu(111). *J. Catal.* **2008**, 258 (1), 44-51.
(73) Wang, Y.; Kattel, S.; Gao, W.; Li, K.; Liu, P.; Chen, J. G.; Wang, H., Exploring the ternary interactions in Cu-ZnO-ZrO_2 catalysts for efficient CO_2 hydrogenation to methanol. *Nat. Commun.* **2019**, 10.
(74) Lustemberg, P. G.; Palomino, R. M.; Gutierrez, R. A.; Grinter, D. C.; Vorokhta, M.; Liu, Z.; Ramirez, P. J.; Matolin, V.; Veronica Ganduglia-Pirovano, M.; Senanayake, S. D.; Rodriguez, J. A., Direct Conversion of Methane to Methanol on Ni-Ceria Surfaces: Metal-Support Interactions and Water-Enabled Catalytic Conversion by Site Blocking. *J. Am. Chem. Soc.* **2018**, 140 (24), 7681-7687.
(75) Kung, H. H., Deactivation of methanol synthesis catalysts-a review. *Catal. Today* **1992**, 11 (4), 443-453.
(76) Saito, M.; Fujitani, T.; Takeuchi, M.; Watanabe, T., Development of copper/zinc oxide-based multicomponent catalysts for methanol synthesis from carbon dioxide and hydrogen. *Appl. Catal., A* **1996**, 138 (2), 311-318.
(77) Michiels, R.; Engelmann, Y.; Bogaerts, A., Plasma Catalysis for CO_2 Hydrogenation: Unlocking New Pathways toward CH_3OH. *J. Phys. Chem. C* **2020**, 124 (47), 25859-25872.
(78) Butterworth, T.; Elder, R.; Allen, R., Effects of particle size on CO_2 reduction and discharge characteristics in a packed bed plasma reactor. *Chem. Eng. J.* **2016**, 293, 55-67.
(79) Van Laer, K.; Bogaerts, A., Fluid modelling of a packed bed dielectric barrier discharge plasma reactor. *Plasma Sources Sci Technol* **2016**, 25 (1), 015002.
(80) Jafarzadeh, A.; Bal, K. M.; Bogaerts, A.; Neyts, E. C., CO_2 Activation on TiO_2-Supported Cu_5 and Ni_5 Nanoclusters: Effect of Plasma-Induced Surface Charging. *J. Phys. Chem. C* **2019**, 123 (11), 6516-6525.
(81) Jafarzadeh, A.; Bal, K. M.; Bogaerts, A.; Neyts, E. C., Activation of CO_2 on Copper Surfaces: The Synergy between Electric Field, Surface Morphology, and Excess Electrons. *J. Phys. Chem. C* **2020**, 124 (12), 6747-6755.
(82) Quan, J.; Muttaqien, F.; Kondo, T.; Kozarashi, T.; Mogi, T.; Imabayashi, T.; Hamamoto, Y.; Inagaki, K.; Hamada, I.; Morikawa, Y.; Nakamura, J., Vibration-driven reaction of CO_2 on Cu surfaces via Eley-Rideal-type mechanism. *Nat. Chem.* **2019**, 11 (8), 722-729.